

Diffusion and localization in quantum random resistor networks

Gerald Schubert¹ and Holger Fehske¹

¹*Institut für Physik, Ernst-Moritz-Arndt Universität Greifswald, 17487 Greifswald, Germany*

(Dated: November 13, 2018)

The theoretical description of transport in a wide class of novel materials is based upon quantum percolation and related random resistor network (RRN) models. We examine the localization properties of electronic states of diverse two-dimensional quantum percolation models using exact diagonalization in combination with kernel polynomial expansion techniques. Employing the local distribution approach we determine the arithmetically and geometrically averaged densities of states in order to distinguish extended, current carrying states from localized ones. To get further insight into the nature of eigenstates of RRN models we analyze the probability distribution of the local density of states in the whole parameter and energy range. For a recently proposed RRN representation of graphene sheets we discuss leakage effects.

PACS numbers: 71.23.An, 71.30.+h, 05.60.Gg, 72.15.Rn

I. INTRODUCTION

Disorder is an intrinsic feature of many solid state materials. The spatial inhomogeneity of a sample strongly affects the transport properties, particularly in low-dimensional systems where Anderson localization effects play an important role¹. Attempts to describe quantum transport in disordered media usually rely on free electron models with random links between lattice sites and/or varying on-site potentials. Then transport is related to percolating current patterns in a kind of random resistor network (RRN). RRN models apply to both classical and quantum percolation problems. For classical percolation the existence of a sample-spanning cluster ensures finite conductivity above a certain percolation threshold of accessible sites p_c . In the quantum case, the appearance of current carrying states strongly depends on the (relative) importance of tunneling, scattering and interference processes. For instance, strong scattering at the irregular boundaries of a conducting cluster may lead to a localization of the charge carrier even for $p > p_c$.

Over the past years percolation approaches have been employed in many circumstances, e.g., in order to model the transport properties of doped semiconductors² and granular metals³, the dynamics of atomic Fermi-Bose mixtures⁴, the wave propagation through binary inhomogeneous media⁵, as well as the formation of novel two-dimensional spin liquids⁶. Another focal point is the metal-insulator transition, e.g., in 2D n-GaAs heterostructures⁷ and colossal magnetoresistive manganite films⁸, or rather the superconductor-insulator and (integer) quantum Hall transitions^{9,10}. Quite recently, the problem of disorder in systems with Dirac fermions has been studied in the context of dirty superconductors¹¹ and two-dimensional (2D) graphene^{12,13,14,15}.

In mono- and bilayer graphene, and graphene-based field effect transistors, strong fluctuations of the local charge density and, thus, the local conductivity have been reported near the so-called “neutrality point”^{16,17,18,19}, where the conductivity reaches its minimum. The mesoscopic regions of different charge car-

rier density may be caused by inhomogeneities in the substrate, or non-perfect stacking^{20,21,22,23}. In order to model the minimal conductivity in graphene a RRN representation of a graphene sheet has been proposed by Cheianov *et al.*²⁴, where random links between electron and hole “puddles” (corresponding to lattice sites) are assumed to determine the observable conductivity rather than the local conductivity of a puddle. Such a RRN formulated on a square lattice is closely related to a 2D quantum percolation percolation model with additional finite “leakage” between all lattice sites.

Motivated by this situation, in this paper we perform an in-depth numerical study of generalized 2D percolative RRN models. In particular we analyze how the leakage and connectivity rules influence the nature of the single-particle states. Since in two dimensions the problem of quantum percolation is still discussed controversially—especially with respect to the existence of a quantum percolation threshold $p_c \leq p_q \leq 1$, see, e.g., Refs. 25,26,27,28,29,30,31,32,33,34,35,36—we rely on unbiased numerical techniques, which take quantum effects fully into account. To this end we employ the so-called local distribution (LD) approach^{37,38}. This technique, based on the determination of the distribution of the local density of states (LDOS) for all energies, has been previously applied to tackle localization phenomena in various disordered systems with great success^{39,40,41,42,43,44,45,46}.

The paper is organized as follows. Sect. II introduces the RRN model and briefly outlines the LD approach. In Sect. III, we examine the localization properties of the eigenstates of RRN models by calculating the LDOS distribution, as well as the average and typical density of states. Sect. IV contains our conclusions.

II. MODEL AND METHODS

Let us consider a 2D square lattice with N sites on two sub-lattices α and β , which, e.g., might represent regions of different charge carrier concentrations. The sub-lattices are linked by connection rules characteris-

tic of specific materials. Generation rule A corresponds to a checkerboard-like structure (see upper left panel of Fig. 1). Regions (sites) of the sub-lattices are randomly connected with each other (lower panels of Fig. 1) according to the connection rules displayed in the upper right panel of Fig. 1. The hopping probability between suchlike connected sites is assumed to be much higher than for hopping events to nearest neighbors. The latter ones are reduced by the leakage $\lambda < 1$.

For the more abstract case of generation rule B (with the above connection rule), additional random bonds connect α to β sites, favoring the formation of quasi one-dimensional zig-zag chains. We still have a weak leakage between all neighboring sites. This generation rule can be interpreted as an attempt to incorporate a spatial anisotropy into the model.

In both cases, the corresponding RRN can be described by the Hamiltonian

$$\begin{aligned}
 H = -t & \left[\sum_{i \in \alpha} \left(\eta_i c_i^\dagger c_{i+\nearrow} + (1 - \eta_i) c_{i+\uparrow}^\dagger c_{i+\rightarrow} \right) \right. \\
 & + \sum_{i \in \beta} \left(\eta_i c_{i+\uparrow}^\dagger c_{i+\rightarrow} + (1 - \eta_i) c_i^\dagger c_{i+\nearrow} \right) \\
 & \left. + \lambda \sum_i \left(c_i^\dagger c_{i+\rightarrow} c_{i+\uparrow}^\dagger c_{i+\uparrow} \right) \right] + \text{H.c.} .
 \end{aligned} \quad (1)$$

Here c_i^\dagger (c_i) creates (annihilates) an electron at site i and the arrows denote the nearest neighbors site of i in the corresponding direction. The discrete random variables $\eta_i \in \{0, 1\}$ determine which diagonal in the plaquette is connected (cf. upper right panel in Fig. 1). By fixing the expectation value of the $\{\eta_i\}$ -distribution, $p = \langle \eta_i \rangle$, we can control the sizes of the regions of connected lattice sites. For $p = 0.5$ the RRN model (1) does not depend on the generation rules A or B because of the symmetry of the bimodal $\{\eta_i\}$ -distribution. In the limit of vanishing leakage we obtain the standard 2D quantum percolation model using generation rule A.

To characterize the transport behavior of our model we adopt the local distribution approach (for a detailed description of this technique, we refer the reader to Ref. 47 and references therein). The main idea is the following: We calculate the LDOS for all lattice sites i ,

$$\rho_i(E) = \sum_{n=1}^N |\langle i|n\rangle|^2 \delta(E - E_n) . \quad (2)$$

This quantity depends on the energy and varies from site to site. Moreover the ρ_i are specific for a particular sample (realization $\{\eta_i\}$). Calculating and recording ρ_i for many sites and realizations we obtain the probability distribution $f[\rho_i]$ and distribution function

$$F[\rho_i] = \int_0^{\rho_i} f[\rho'_i] d\rho'_i . \quad (3)$$

of $\{\rho_i\}$. Both $f[\rho_i]$ and $F[\rho_i]$ are self-averaging. That is, in the thermodynamic limit, they are independent of the

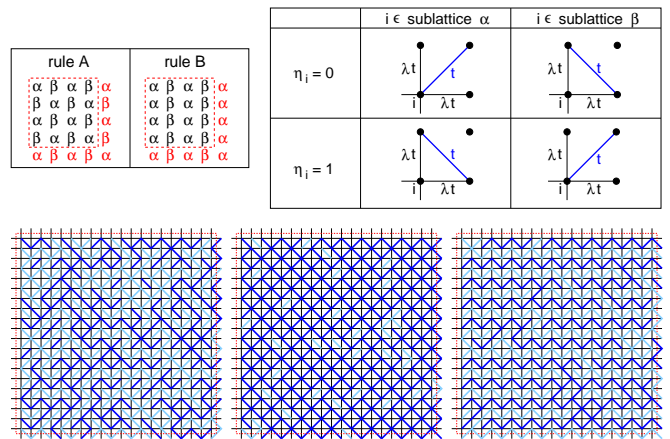


FIG. 1: (Color online) Upper left panel: Generation rules A and B for sub-lattices α and β . Upper right panel: Connection rule of neighboring sites on different sub-lattices. Lower panels: Three particular cluster realizations representing the above rules on a 20×20 lattice. From left to right: $p = 0.50$, $p = 0.90$ (rule A), $p = 0.90$ (rule B). Note that rules A and B become equivalent for $p = 0.50$. At the red dashed lines the system is interconnected by periodic boundary conditions.

actual realization $\{\eta_i\}$ and the chosen sites $\{i\}$, but will be solely determined by the (global) model parameters p , λ , and the generation rule. This restores translational invariance on the level of distributions.

A well-established criterion for localization then can be deduced from the shape of the distribution function. Since for an extended (current carrying) state the amplitude of the wave function is more or less uniform, $F[\rho_i]$ steeply rises in the vicinity of the mean value of the LDOS, $\rho_{\text{me}} = \langle \rho_i \rangle$. For localized states, on the other hand, the LDOS strongly fluctuates throughout the lattice leading to a rather gradual increase of $F[\rho_i]$ as a function of the magnitude of ρ_i . To capture this different behavior quantitatively, we may compare the arithmetic mean of the LDOS, ρ_{me} , to its the geometric mean, the so-called “typical” DOS, $\rho_{\text{ty}} = e^{\langle \ln(\rho_i) \rangle}$, see, e.g., Ref. 39.

For extended states ρ_{me} and ρ_{ty} are of the same order, whereas ρ_{ty} vanishes for a localized state (or, in a finite system, is at least considerably suppressed). Of course, a reliable distinction between extended and localized states requires the consideration of different system sizes. For extended states $F[\rho_i]$ is independent of N . By contrast, for localized states $F[\rho_i]$ shifts toward lower values as N increases (causing the reduced value of ρ_{ty}).

The LDOS can be calculated very efficiently by means of the kernel polynomial method (KPM)⁴⁸. Within this technique, the spectrum of H is expanded into a finite series of Chebyshev polynomials with additional damping factors. This approximation can be viewed as a convolution of the spectrum with the Jackson kernel, an almost Gaussian of width σ . As σ depends on the order of the Chebyshev series as well as on the energy, we have to adapt the expansion order to ensure a uniform resolu-

tion (constant σ) for the whole spectrum⁴⁷.

III. RESULTS

In Fig. 2 we compare the mean and typical DOS in dependence on λ and p for generation rules A and B. While the 2D percolation model ($\lambda = 0$, rule A) exhibits symmetric DOS spectra, the inclusion of next-nearest neighbor hopping causes an asymmetry that grows with increasing λ . Moreover, if $p > 0.5$, the results obtained for the two generation rules differ significantly. For the A-case the mean DOS resembles the 2D DOS. Generation rule B leads to a spectrum evocative of the DOS in 1D. In both cases a multitude of spikes exists which we can attribute to localized states on “isolated” islands. This feature is well known from the binary alloy model⁴⁹. Increasing the leakage broadens the peaks and reduces their abundance, because the “isolation” of the islands is weakened. Furthermore, the leakage shifts the “special energies” at which these peaks appear toward lower values as compared to those in the standard 2D percolation model⁴⁹.

The typical DOS underlines the prominent role of the leakage. In Fig. 2 (a) a vanishing ρ_{ty} suggests that all states are localized. As long as the leakage is very small,

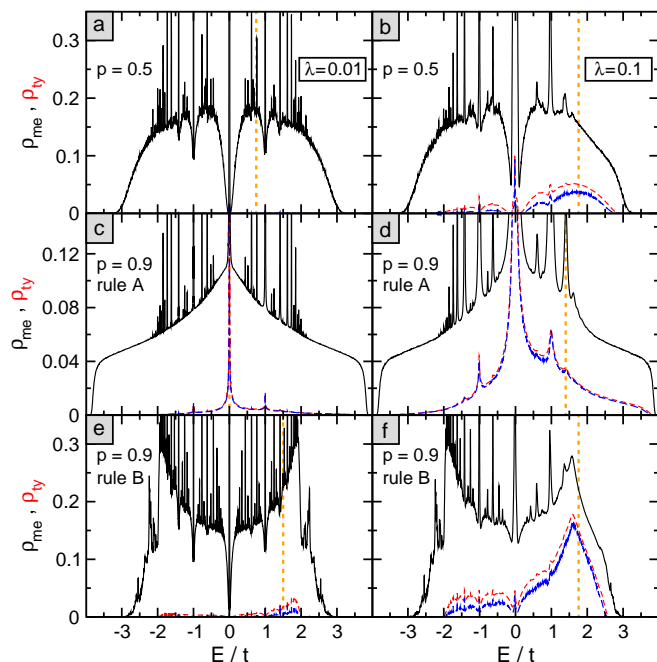


FIG. 2: (Color online) Mean (upper solid lines) and typical (lower dashed lines) DOS. Results are shown for $N = 400^2$ and $N\sigma = 45$ for different p , λ and generation rules A and B. To illustrate the finite-size dependence of ρ_{ty} the results for a $N = 800^2$ lattice are included (long dashed lines). The data are based on 10^5 (10^4) individual LDOS spectra for $N = 400^2$ (800^2). Dotted vertical lines indicate the energies for which the distribution functions of the LDOS are given in Fig. 3.

the typical DOS remains small as well throughout the band. This also holds for larger p and both generation rules. Sizeable values of ρ_{ty} appear at larger values of λ only (compare the data for $\lambda = 0.01$ and 0.1). As for the mean DOS, we observe a pronounced asymmetry of ρ_{ty} in the electronic band. This favors a finite typical DOS, i.e. extended states, for $E > 0$. However, this has to be taken with caution. If we increase the system size together with the resolution of the KPM in such a way, that the number of states within the width of the Jackson kernel, $N\sigma$, is kept constant, the picture changes. While for truly extended states, ρ_{ty} should be independent of the system size (cf. Fig. 2 (d)), in Figs. 2 (b) and (f), the typical DOS decreases with increasing system size. This points towards a large localization length. While for small and moderate N the state still spans the entire lattice, the system size exceeds the localization length for larger N . Therefore, on a considerable number of sites the LDOS is very small, leading to a reduced value of ρ_{ty} . Then the question arises, why in panel Fig. 2 (d) the typical DOS is reduced as compared to ρ_{me} , even though this ratio is independent of N . This can be easily understood if we consider a perfectly ordered system, i.e. $p = 1$. There the sites which do not belong to the spanning sublattice are also taken into account, and amount to half of the lattice sites. In absence of leakage, at those sites the LDOS vanishes and probing such a site completely suppresses ρ_{ty} . For finite λ , however, these sites have small amplitudes and in this manner ρ_{ty} is reduced as compared to ρ_{me} but finite. These arguments also hold for panel Fig. 2 (b), but there the low leakage suppresses the typical DOS already almost completely, except for $E = 0$.

As mentioned above, the comparison of ρ_{ty} and ρ_{me} may only serve as a first indication of localization. A careful finite-size scaling of the full probability function (or the distribution function) of the LDOS allows for a more reliable distinction between extended and localized states. Thereto, in Fig. 3 we show for the same sets of parameters the distribution function of the LDOS at various characteristic energies. In the panels of Fig. 2 these energies are indicated by vertical dotted lines.

Here one crucial point concerns the normalization of ρ_i to ρ_{me} . For a completely extended state, with uniform amplitudes, the distribution function would be a step function. Due to the used scaling, this step would be located at $\rho_i/\rho_{\text{me}} = 1$, irrespective of the system size. The random structure of the underlying lattice will distort this perfect jump-like behavior of $F[\rho_i/\rho_{\text{me}}]$. But nevertheless extended states are characterized by an N -independent distribution function [cf. Fig. 3 (d)]. In contrast, for localized states, $F[\rho_i/\rho_{\text{me}}]$ constantly shifts toward lower values as N increases [cf. Figs. 3 (a), (e)]. Depending on the localization length, this effect is more or less pronounced. Thus, a wide range of system sizes is necessary in order to discriminate localized from extended states by means of finite-size scaling [cf. Figs. 3 (b) and (f)].

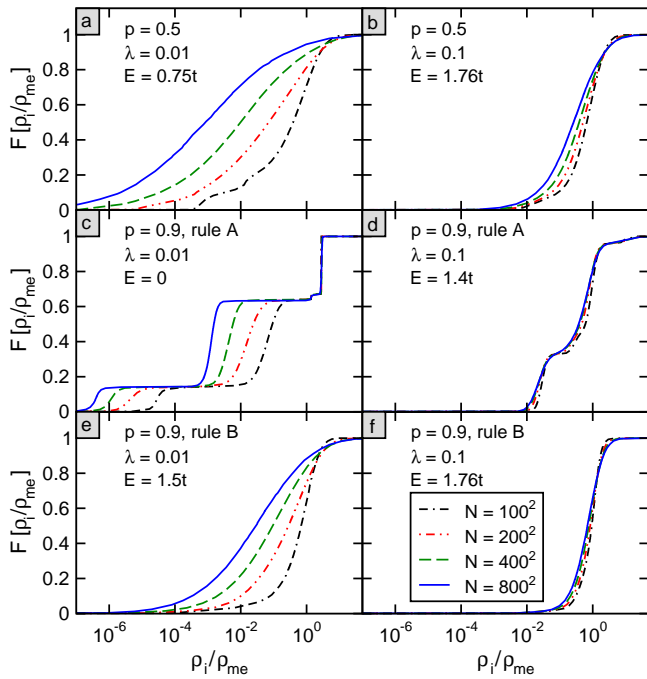


FIG. 3: (Color online) Distribution function of the normalized LDOS for the energies indicated by vertical lines in Fig. 2. The statistics is based on 10^7 , 10^6 , 10^5 , 10^4 LDOS values for $N = 100^2$, 200^2 , 400^2 , 800^2 and resolution $N\sigma = 45$.

A particular interesting shape of $F[\rho_i/\rho_{me}]$ appears in Fig. 3 (c), for a state in the band center. From the multi-step structure, we may deduce that the probability distribution is mainly concentrated around three values. The largest of those values is independent on N , while the others show the above discussed variation. This behavior can be explained by considering again the completely ordered case. In absence of leakage the $E = 0$ eigenstate is highly degenerate: we have $N/2$ completely localized states, one on each isolated site. The other half of the eigenstates are extended in the perfect lattice, providing energies in the whole band. As the LDOS probes the complete eigenspace and not just the amplitude of one particular eigenstate, at $E = 0$ we obtain the same value of ρ_i/ρ_{me} for each isolated site. Introducing a small leakage kills the high degeneracy in principle. Due to the finite energy resolution of the KPM, however, still many of these states contribute to the LDOS at $E = 0$. In the presence of imperfections ($p < 1$), some of the former isolated sites will now be connected to form larger islands. Then less than $N/2$ states will contribute to the “isolated islands” peak at high ρ_i/ρ_{me} [but still around 38% in Fig. 3 (c)]. The second step, having a weight of about 50%, is due to sites on the highly connected majority sub-lattice, on which the LDOS is reduced but finite due to the leakage. The remaining lowest step originates from more complicated islands of several sites. On those islands (2, 3, ... sites), the $E = 0$ eigenstates have vanishing amplitudes on some sites. Due to the leakage these

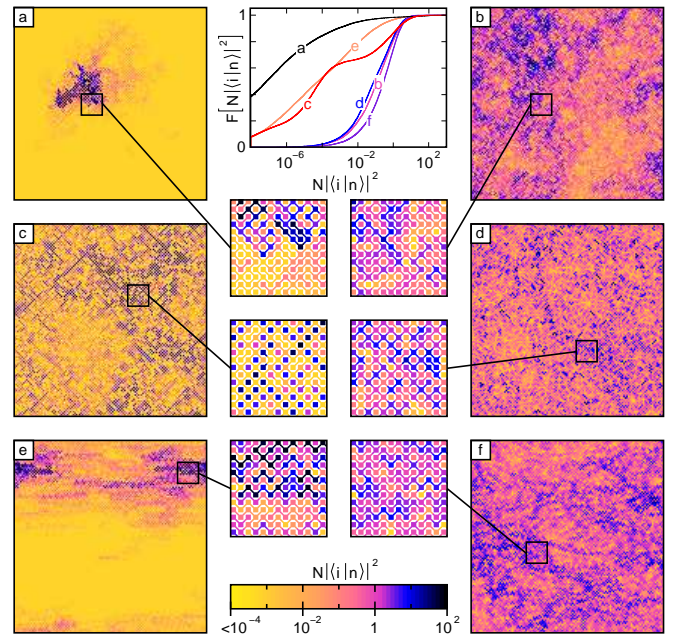


FIG. 4: (Color online) Normalized occupation probability $N|\langle i|n\rangle|^2$ of several characteristic eigenstates $|n\rangle$ on a $N = 128^2$ lattice. The generation rules, doping and leakage as well as the chosen energies E_n correspond to the ones for which the distribution functions of the LDOS has been presented in Fig. 3 (same order of panels). In the center column the distribution function of the normalized occupation probability is shown for these states. Furthermore, for each state an enlargement of a characteristic region together with the local structure of the present links is shown.

sites again acquire a finite value of ρ_i .

To get additional insight into the spatial structure of the eigenstates, we investigate a smaller 128×128 system using exact diagonalization techniques. Figure 4 visualizes characteristic eigenstates for the parameters discussed in Figs. 2 and 3. Most notably is the pronounced leakage-dependence of the results. While we see clear localization for $\lambda = 0.01$ [Fig. 4 (a), (e)], in the high-leakage case all states span the entire lattice. The 1D structure for rule B and large p , which we already found in the DOS in Fig. 2 (e), is also predominant in Fig. 4 (e). In Fig. 4 (c), notably in the magnifying inset, we see our assumption confirmed, that sites with large amplitudes are almost exclusively isolated, with the exception of some larger islands. Having the sharp step in mind, which occurs in Fig. 3 (c) at large ρ_i/ρ_{me} , the alert reader may wonder about the different amplitudes in Fig. 4 (c) and the rather smooth increase of $F[N|\langle i|n\rangle|^2]$ in the middle column. This discrepancy is again due to the high degeneracy of the $E = 0$ state and the fact, that the LDOS takes into account the whole $E = 0$ eigenspace. In contrast, for $N|\langle i|n\rangle|^2$, we randomly pick one particular eigenstate out of this subspace. For the other $E = 0$ eigenstates, $F[N|\langle i|n\rangle|^2]$ looks similar, only the location of the sites with maximum amplitudes differ. Clearly, the

physically relevant quantity is the LDOS, as the choice of eigenvectors which span the eigenspace is arbitrary up to any linear combinations of them. Summing up all eigenstates to $E = 0$ for a fixed lattice site we indeed get the same amplitude on each isolated site, which brings us back to the findings of Fig. 3 (c). Finally we consider the case of higher leakage ($\lambda = 0.1$), where all states look rather similar. Here the amplitudes fluctuate over a smaller range, and the fluctuations occur on very short spatial scales. This is most pronounced in Figs. 4 (d), (f) where no global structures can be distinguished, in accordance with the notion of extended states. By contrast, although the state in Fig. 4 (b) spans the entire lattice, we observe sizeable regions with higher and lower amplitudes than the mean value. Presumably, these inhomogeneities are even more pronounced for larger systems which, however, (as yet) are not accessible by our exact diagonalization studies. In any case, the shifting of the LDOS distribution function in Fig. 3 (b) suggests this state to be localized on large length scales.

IV. SUMMARY

In this work we investigated the two-dimensional quantum percolation problem for a broader class of random resistor network models including leakage terms. Com-

paring exact diagonalization, Chebyshev expansion and local distribution approaches in calculating the local density of states, we determine—after a careful finite-size scaling—the localization properties of the single-particle eigenstates. We found that current carrying states exist, and that the appearance of diffusion is mainly triggered by the amount of leakage. In contrast to previous work we analyzed the nature of the single-particle states in the whole energy band and not just the vicinity of the neutrality point in the band center $E = 0$. A tendency toward extended states is observed for $E > 0$. In view of the simplicity of the considered RRN model, our data are certainly not yet suited to be compared against real transport data for, e.g., undoped graphene monolayers. Nevertheless, using unbiased numerics on a microscopic level, we fully account for quantum effects in a RRN model originally designed to describe transport in a graphene-based field effect transistor, and received results that support a minimal conductivity in graphene.

Acknowledgments

The numerical calculations have been performed on the HLRB at LRZ Munich and the TeraFlop compute cluster at the Institute of Physics, Greifswald University.

-
- ¹ P. W. Anderson, Phys. Rev. **109**, 1492 (1958).
² M. Inui, S. A. Trugman, and E. Abrahams, Phys. Rev. B **49**, 3190 (1994).
³ M. V. Feigel'mann, A. Ioselevich, and M. Skvortsov, Phys. Rev. Lett. **93**, 136403 (2004).
⁴ A. Sanpera, A. Kantian, L. Sanchez-Palencia, J. Zakrzewski, and M. Lewenstein, Phys. Rev. Lett. **93**, 040401 (2004).
⁵ Y. Avishai and J. Luch, Phys. Rev. B **45**, 1974 (1992).
⁶ R. Yu, T. Roscilde, and S. Haas, Phys. Rev. Lett. **94**, 197204 (2005).
⁷ S. Das Sarma, M. P. Lilly, E. H. Hwang, L. N. Pfeiffer, K. W. West, and J. L. Reno, Phys. Rev. Lett. **94**, 136401 (2005).
⁸ T. Becker, C. Streng, Y. Luo, V. Moshnyaga, B. Damaschke, N. Shannon, and K. Samwer, Phys. Rev. Lett. **89**, 237203 (2002).
⁹ Y. Dubi, Y. Meir, and Y. Avishai, Phys. Rev. B **71**, 125311 (2005).
¹⁰ N. Sandler, H. R. Maei, and J. Kondev, Phys. Rev. B **70**, 045309 (2004).
¹¹ P. J. Hirschfeld and W. A. Atkinson, J. Low Temp. Phys. **126**, 881 (2002).
¹² V. M. Pereira, F. Guimea, J. M. B. Lopes dos Santos, N. M. R. Peres, and A. H. Castro Neto, Phys. Rev. Lett. **96**, 036801 (2006).
¹³ I. Martin and Y. M. Blanter (2007), preprint, URL [arXiv:0705.0532](https://arxiv.org/abs/0705.0532).
¹⁴ S.-J. Xiong and Y. Xiong, Phys. Rev. B **76**, 214204 (2007).
¹⁵ A. Rycerz, J. Tworzydło, and C. W. J. Beenakker, Europhys. Lett. **79**, 57003 (2007).
¹⁶ K. S. Novoselov, E. McCann, S. V. Morozov, V. I. Fal'ko, M. I. Katsnelson, U. Zeitler, D. Jiang, F. Schedin, and A. K. Geim, Nature Phys. **2**, 177 (2006).
¹⁷ S. Cho and M. S. Fuhrer (2007), preprint, URL [arXiv:0705.3239](https://arxiv.org/abs/0705.3239).
¹⁸ J. Martin, N. Akerman, G. Ulbricht, T. Lohmann, J. H. Smet, K. von Klitzing, and A. Yacoby, Nature Phys. **4**, 144 (2008).
¹⁹ M. I. Katsnelson, K. S. Novoselov, and A. K. Geim, Nature Phys. **2**, 620 (2006).
²⁰ E. Rossi and S. Das Sarma (2008), preprint, URL [arXiv:0803.0963](https://arxiv.org/abs/0803.0963).
²¹ Y.-W. Tan, Y. Zhang, K. Bolotin, Y. Zhao, S. Adam, E. H. Hwang, S. Das Sarma, H. L. Stormer, and P. Kim, Phys. Rev. Lett. **99**, 246803 (2007).
²² J. H. Chen, C. Jang, M. S. Fuhrer, E. D. Williams, and M. Ishigami (2007), preprint, URL [arXiv:0708.2408](https://arxiv.org/abs/0708.2408).
²³ M. I. Katsnelson and A. K. Geim (2007), preprint, URL [arXiv:0706.2490](https://arxiv.org/abs/0706.2490).
²⁴ V. V. Cheianov, V. I. Fal'ko, B. L. Altshuler, and I. L. Aleiner, Phys. Rev. Lett. **99**, 176801 (2007).
²⁵ G. Schubert and H. Fehske, Phys. Rev. B **77**, 245130 (2008).
²⁶ C. M. Soukoulis and G. S. Grest, Phys. Rev. B **44**, 4685 (1991).
²⁷ A. Mookerjee, I. Dasgupta, and T. Saha, Int. J. Mod. Phys. B **9**, 2989 (1995).
²⁸ A. Bunde, J. W. Kantelhardt, and L. Schweitzer, Ann. Phys. (Leipzig) **7**, 372 (1998).

- ²⁹ G. Haldas, A. Kolek, and A. W. Stadler, *Phys. Status Solidi B* **230**, 249 (2002).
- ³⁰ T. Odagaki and K. C. Chang, *Phys. Rev. B* **30**, 1612 (1984).
- ³¹ V. Srivastava and M. Chaturvedi, *Phys. Rev. B* **30**, 2238 (1984).
- ³² M. Letz and K. Ziegler, *Philos. Mag. B* **79**, 491 (1999).
- ³³ D. Daboul, I. Chang, and A. Aharony, *Eur. Phys. J. B* **16**, 303 (2000).
- ³⁴ A. Eilmes, R. A. Römer, and M. Schreiber, *Physica B* **296**, 46 (2001).
- ³⁵ H. N. Nazareno, P. E. de Brito, and E. S. Rodrigues, *Phys. Rev. B* **66**, 012205 (2002).
- ³⁶ M. F. Islam and H. Nakanishi (2007), preprint, URL [arXiv:0709.4085](https://arxiv.org/abs/0709.4085).
- ³⁷ A. Alvermann and H. Fehske, *J. Phys.: Conf. Ser.* **35**, 145 (2006).
- ³⁸ A. Alvermann and H. Fehske, *Lecture Notes in Physics* **739**, 505 (2008).
- ³⁹ G. Schubert, A. Weiße, G. Wellein, and H. Fehske, in *High Performance Computing in Science and Engineering, Garching 2004*, edited by A. Bode and F. Durst (Springer-Verlag, Heidelberg, 2005), pp. 237–250.
- ⁴⁰ V. Dobrosavljević, A. A. Pastor, and B. K. Nikolić, *Europhys. Lett.* **62**, 76 (2003).
- ⁴¹ A. Alvermann, G. Schubert, A. Weiße, F. X. Bronold, and H. Fehske, *Physica B* **359–361**, 789 (2005).
- ⁴² G. Schubert, A. Weiße, and H. Fehske, *Physica B* **359–361**, 801 (2005).
- ⁴³ V. Dobrosavljević and G. Kotliar, *Phys. Rev. Lett.* **78**, 3943 (1997).
- ⁴⁴ K. Byczuk, W. Hofstetter, and D. Vollhardt, *Phys. Rev. Lett.* **94**, 056404 (2005).
- ⁴⁵ F. X. Bronold and H. Fehske, *Phys. Rev. B* **66**, 073102 (2002).
- ⁴⁶ F. X. Bronold, A. Alvermann, and H. Fehske, *Philos. Mag.* **84**, 673 (2004).
- ⁴⁷ G. Schubert and H. Fehske, *Lecture Notes in Physics* **xxx**, xxx (2008).
- ⁴⁸ A. Weiße, G. Wellein, A. Alvermann, and H. Fehske, *Rev. Mod. Phys.* **78**, 275 (2006).
- ⁴⁹ G. Schubert, A. Weiße, and H. Fehske, *Phys. Rev. B* **71**, 045126 (2005).